Galactic Dynamics in the Era of Large Surveys
Proceedings IAU Symposium No. 353, 2019
M. Valluri, & J. A. Sellwood

DOI: 00.0000/X000000000000000X

Structure and dynamics of high-z galaxies

Stijn Wuyts[1] and Natascha M. Förster Schreiber[2]

[1]Dept. of Physics, University of Bath,
Claverton Down, Bath, BA2 7AY, UK
email: s.wuyts@bath.ac.uk

[2]Max-Planck-Institut für extraterrestrische Physik,
Giessenbachstr. 1, Garching, D-85737, Germany
email:forster@mpe.mpg.de

Abstract. HST and integral-field spectroscopic observations of star-forming galaxies at cosmic noon provide a view on the spatial distribution of stars, gas and dust, and probe gaseous motions revealing the central gravitational potential and local feedback processes at play. In this paper, we review recent insights gained from such observations, with an emphasis on results obtained through near-infrared imaging spectroscopy. Their context and implications are documented more fully in a forthcoming review article by Förster Schreiber & Wuyts (in prep).

Keywords. Galaxies: structure, Galaxies: kinematics, Galaxies: high-redshift

1. Introduction

Census. Accumulating over more than a decade, a large cross section of the galaxy evolution community has contributed to assembling a wedding cake of deep legacy fields from which consistent multi-wavelength photometric catalogs have been extracted and made publicly available. Ranging from ultra-deep pencil-beam surveys such as the Hubble XDF to areas of 2 deg^2 (COSMOS) and beyond (e.g., Hyper-SuprimeCam, VIDEO, KIDS+Viking) they complement each other in a balancing of area versus depth.

Another dimension along which legacy lookback surveys have advanced and augmented the potential to infer physical properties of galaxies is wavelength, both in its coverage and sampling. For example, the intermediate $R \sim 13 - 130$ SED sampling provided by slitless grism spectroscopy (e.g., 3D-HST) enabled a sensitive improvement in redshift estimates. These in their turn allowed the selection of specifically those targets for follow-up IFU spectroscopy that have their emission lines of interest redshifted away from OH sky lines that render significant swathes of the near-infrared wavelength regime unsuitable for detailed line profile analyses as discussed in Section 3 (Wisnioski et al. 2015).

These rich multi-wavelength data facilitated a mass-complete census of star-forming and quiescent galaxies over more than 90% of cosmic history (e.g., Davidzon et al. 2017).

Scaling relations. Alongside an improved census of the number of galaxies as a function of mass, redshift and type (star-forming/quiescent) multi-wavelength lookback surveys have helped establish the regularity of galaxy properties across cosmic time. This regularity is captured by a set of scaling relations aimed at describing the star-forming galaxy (SFG) population as a one-parameter family. At any given epoch, physical properties of SFGs such as their star formation rate (SFR), gas content, metallicity, rotational velocity and size can be parameterized as a function of galaxy stellar mass. The change in zero point, slope and/or shape of such scaling relations then encodes their evolution in a population averaged sense (Speagle et al. 2014; Tacconi et al. 2018; Sanders et al. 2018; Übler et al. 2017; van der Wel et al. 2014).

Evolution. The evolution of population-averaged physical properties evaluated at fixed

mass does not equate to the evolution of individual galaxies, which grow in mass over time. In recent years, considerable efforts have therefore gone into reconstructing the growth history of individual systems. Perhaps the most common approach of connecting progenitor and descendant galaxies across cosmic time consists of assuming that their relative mass ranking remains preserved (i.e., the most massive galaxy today was also the most massive at earlier epochs and so on), in which case progenitors and descendants can be considered to live at the same comoving number density. Curves of stellar mass growth as a function of redshift can then be combined with the aforementioned scaling relations to establish how an individual galaxy consumes its gas, enriches its ISM, grows its size and builds up angular momentum.

For a galaxy of Milky Way mass today, it reveals the so-called era of cosmic noon ($1 < z < 3$) as a key epoch during which the star formation activity peaked, the gas richness dropped most dramatically (despite continuing yet declining gaseous accretion onto the galaxy) and the chemical enrichment proceeded most quickly. In relative terms, the rate of size growth was maintained over a much more extended period of time down to the present day and much of the stellar total angular momentum build-up happened at later times (see Figure 1 of Förster Schreiber & Wuyts in prep).

Toward a multi-wavelength resolved view of galaxies at cosmic noon. While highlighting the importance of the cosmic noon era to understand the growth history of Milky Way and higher mass galaxies, the above galaxy-integrated quantities need to be paired with a resolved view of their structure and kinematics if we are to understand the physical drivers behind their evolution. With multi-band resolved maps of thousands of distant galaxies in the rest-UV to optical, resolved observations of ionized gas line emission in hundreds of them (thousands if relying on stacking of low-S/N Hα maps from HST grism spectroscopy out to $z < 1.5$), and far-infrared continuum and molecular gas emission line maps for dozens, the field is increasingly moving towards such spatially resolved, multi-tracer analyses. In this paper, we review key insights gained from high-resolution imaging campaigns (Section 2) as well as imaging spectroscopy, with dynamics offering a probe of the gravitational potential and non-gravitational motions complementing metallicity gradients as diagnostics of the feedback processes at play (Section 3). Finally, we present an outlook to new instrumentation and facilities projected to come on-line in the next decade and enabling the tackling of a number of remaining open questions (Section 4).

2. Lessons from high-resolution imaging

Deep HST/WFC3 imaging of the CANDELS fields and more recent wide-area extensions over as much as 0.6 square degrees (COSMOS-DASH) provide a means to characterize the rest-optical structure of galaxies spanning a large dynamic range in mass out to cosmic noon. van der Wel et al. (2014) characterize the size growth of SFGs at fixed mass to proceed as $\propto (1+z)^{-0.75}$ and of quiescent galaxies as $\propto (1+z)^{-1.48}$, with no appreciable evolution in the slope of the size - mass relation for either of the two types. Parameterized as a function of the Hubble parameter ($R_e(z) \propto H(z)^{-2/3}$), the size growth at fixed mass is consistent with the halo size evolution at fixed halo mass, validating a basic assumption underpinning virtually all semi-analytical models for galaxy formation, namely that the baryons accreted onto a galaxy disk inherit the specific angular momentum of their dark matter haloes (Mo, Mao & White 1998). A follow-up analysis by Huang et al. (2017) of the galaxy size - halo size relation, inferred from tying the empirical size - mass relation with abundance matching results, arrives at similar conclusions, which are also echoed by direct, kinematic measurements of the angular momentum distribution of galaxies out to $z \sim 2.5$ (Burkert et al. 2016). In the

same Mo, Mao & White (1998) formalism for disk formation, the distribution of halo spin parameters found in dark matter simulations is by itself sufficient to account for the observed scatter in galaxy sizes at a given mass (Bullock et al. 2001; Kravtsov 2013) and has more recently even been argued to be too large, requiring an alteration of disk growth in extreme spin parameter halos or a different formalism altogether (Zanisi et al. 2019).

The half-light radius of a galaxy by itself does not capture its structure fully. A 1st order additional specification considers the profile shape, as parameterized by the Sersic index n. It is well known that at all times star-forming and quiescent galaxies differ in their Sersic index distributions, with quiescent galaxies featuring cuspier, more centrally concentrated surface brightness distributions (e.g., Wuyts et al. 2011). As a consequence, the relative distribution of SFGs and quiescent galaxies in the size - mass plane is altered when defining galaxy size based on an aperture containing a different percentage than 50% of the light. This is explored in more depth by Mowla et al. (2019), who leverage the improved number statistics at the massive end provided by COSMOS-DASH, and find SFGs and quiescent galaxies to occupy the same size - mass relation when adopting R_{80} (the radius within which 80% of the light is enclosed) as size definition. They argue it is this size, comprising the bulk of the stars, that relates most tightly to the virial radius of the parent halo ($R_{80} = 0.047\ R_{\rm vir}$), for both galaxy types and across mass and redshift.

3. Lessons from integral-field spectroscopy

The three-dimensional data cubes produced by IFU spectrographs offer a wealth of information extending beyond the valuable mapping of star formation (through Hα) and ISM conditions (through strong rest-optical line ratios). Here, we focus on aspects of the internal dynamics and probes of galactic-scale feedback. The results are largely drawn from the KMOS$^{\rm 3D}$ programme, the survey design and data release of which is documented by Wisnioski et al. (2015, 2019). KMOS$^{\rm 3D}$ combines deep integrations (from 5 hours at $z \sim 0.9$ to a median of 8.7 hours at $z \sim 2$) for a large number of galaxies (740 in total), spanning a wide dynamic range in star formation rate and mass, and targeting a consistent range of rest-wavelengths across the $0.6 < z < 2.7$ portion of cosmic history.

The mass budget of galaxies since cosmic noon. The ubiquity of ordered rotational motions observed in distant SFGs allows the gaseous kinematic moment maps to be employed to dynamically place constraints on the (total) amount of enclosed mass within the disk regions of distant galaxies. To this end, two aspects are of particular concern regarding the analysis of velocity and velocity dispersion profiles of galaxies in the early Universe relative to those observed nearby. First, beam smearing effects can often be severe in seeing limited observations, with a typical galaxy size to beam size ratio of 1.7 in the KMOS$^{\rm 3D}$ sample. Different approaches have been employed in the literature, ranging from a simple rescaling of the galactocentric radius axis accounting for an addition of the PSF size in quadrature (Tiley et al. 2019), to the application of a lookup table with correction factors or a scaling relation based on toy model galaxies to the convert observed to intrinsic rotational velocities and derive an intrinsic velocity dispersion (e.g., Burkert et al. 2016; Johnson et al. 2018), to finally carrying out a forward modeling of the observed velocity and dispersion profiles simultaneously with rotating disk models that are mock observed under the appropriate inclination and beam smearing conditions (e.g., Cresci et al. 2009; Wuyts et al. 2016).

While beam smearing reduces the intrinsic rotational velocity leaving only an imprint in the form of an artificially enhanced observed central velocity dispersion, the presence of local random motions (often referred to as the intrinsic velocity dispersion σ_0) revealed as a plateau to the dispersion profile can on its turn impact the observed rotation curve,

irrespective of beam smearing effects. Such a component of pressure support has the net effect of reducing the rotational velocity with respect to the circular velocity needed to balance a dynamically cold and hence thin disk against gravity ($v_{\rm rot}^2 = v_{\rm circ}^2 - 2\sigma_0 \left(\frac{r}{R_d}\right)$ following Burkert et al. 2010).

Accounting for both effects (beam smearing and contributions from pressure support) when modeling the dynamics of high-redshift gas-rich disks, Wuyts et al. (2016) found higher redshift SFGs, and most notably those featuring the highest surface densities, to be more baryon dominated (with $\langle f_{\rm bar}(< R_e)\rangle \approx 90\%$) than their more extended and lower redshift counterparts. A comparison to the Illustris cosmological hydro simulation and to a much simpler bath tub model in which disk growth is tied to typical halo growth histories through a set of analytical equations, illustrates that similar trends with galaxy surface density emerge naturally within a ΛCDM context, at least at a qualitative level. Those galaxies in which the baryons managed to assemble within a compact region in the center of the parent dark matter halo naturally feature low contributions from dark matter when quantified within the disk region. Efforts to push measurements of rotation curve shapes out to more than 3 R_e through stacking (Lang et al. 2017) or yet deeper integrations (Genzel et al. 2017) confirm the baryon dominated nature of $z \sim 2$ SFGs, without reliance on assumptions and systematics that may affect the stellar and gas mass estimates in Figure 1 (IMF, $\alpha_{\rm CO}$, ...).

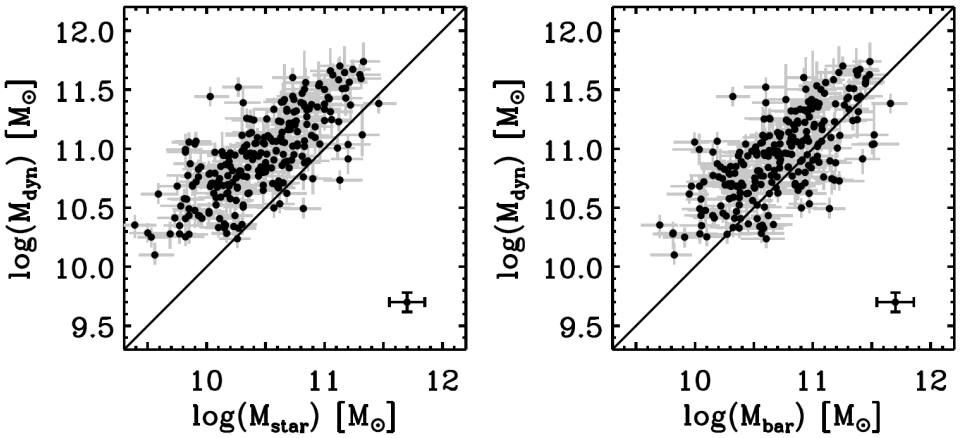

Figure 1. Dynamical mass contrasted to the stellar mass (*left*) and to the baryonic (i.e., stellar + gas) mass (*right*) for 240 KMOS$^{\rm 3D}$ galaxies at $0.6 < z < 2.6$ (reproduced from Wuyts et al. 2016). While the different mass estimates show a clear correlation, they are offset from the one-to-one line and the scatter around the relation is larger than what can be accounted for by measurement uncertainties. The considerable range in redshifts contributes to part of the scatter, with $z \gtrsim 2$ galaxies being more baryon dominated in their disk regions than their lower redshift counterparts. More predictive of the observed stellar-to-dynamical and baryonic-to-dynamical mass ratio still are measures of the galaxies' surface densities. Extended galaxies probe further into their parent halos and hence contain larger dark matter contributions within R_e.

Returning to the reconstruction of evolutionary sequences discussed in Section 1, we recall that the bulk of $z \sim 2$ galaxies in the kinematic samples from KMOS$^{\rm 3D}$ will not evolve into present-day Milky Way-mass systems but will rather end up as higher mass galaxies, predominantly featuring early-type morphologies. If we do not contrast high-z disks to typical spirals in the local Universe, but instead to their more likely early-type descendants, it is noteworthy that those too feature very low dark matter fractions within the confines of their stellar extent (Courteau & Dutton 2015).

Equivalent comparisons between dynamical and stellar masses for galaxies that are already quiescent by cosmic noon have been pursued based on their stellar dynamics. Given their compact sizes, this is most commonly done by means of a virial mass estimator applied to the galaxy-integrated velocity dispersion. In recent years, however, it has become increasingly clear that the quiescent population cannot be treated as purely pressure supported systems, but instead also features substantial amounts of rotational support, as anticipated from a highly dissipational formation process (e.g., Robertson et al. 2006; Wuyts et al. 2010; Wellons et al. 2015). First empirical clues to this end came from a statistical analysis of the axial ratio distribution of early quiescent galaxies, exhibiting a larger number of elongated projected shapes relative to nearby quiescent galaxies (van der Wel et al. 2011; Chang et al. 2013). More recently, the presence of rotational motions and hence need for inclination corrections in deriving dynamical masses was alluded to based on galaxy-integrated dynamical measurements by Belli et al. (2017). Finally, owing to fortuitous lensing magnifications, Newman et al. (2015, 2018) and Toft et al. (2017) were able to spatially resolve the rotation curves of a few $z \sim 2$ quiescent galaxies, placing them on the upper envelope of the distribution of so-called 'fast rotators' among nearby early-type galaxies in angular momentum - ellipticity space. Bezanson et al. (2018) leveraged the larger number statistics from LEGA-C to demonstrate that already at $z \sim 0.8$ a shift toward higher angular momentum quiescent galaxies is notable.

Turbulence in the ISM. Aside from its impact on the inferred dynamical mass budget and the observed rotation curve shapes at cosmic noon, the enhanced levels of turbulence in the ISM of distant galaxies, signaled by a floor to the dispersion profile and parameterized by σ_0, are interesting in their own right. This because it poses the question which process(es) is/are responsible to driving the turbulence and because they can potentially offer an empirical angle on the yet elusive but essential gaseous accretion flows required to continuously replenish the gas-rich high-z disks that feature relatively low depletion times ($t_{\rm dep} \equiv \frac{M_{\rm gas}}{SFR} < 1$ Gyr).

Übler et al. (2019) present the latest compilation of intrinsic velocity dispersion measurements. In the ionized gas phase the level of turbulence progressively increases with redshift, reaching $\sigma_0 \approx 45$ km s^{-1} at $z \sim 2.3$, roughly twice of what is typical for nearby disks. In the cold gas phase, the number of measurements at high redshift is still modest, but early ALMA and NOEMA results suggest a similar increase with redshift, albeit offset downward by 10 - 15 km s^{-1}. In other words, it is not just the ionized gas at 10^4 K that is more easily stirred by the enhanced levels of star formation at cosmic noon. In fact, contrasting their measurements to a theoretical model by Krumholz et al. (2018) they conclude that stellar feedback alone is not capable to explain the full range of σ_0 values observed, and specifically their relation to the galaxies' observed SFR, rotational velocity and gas fraction. Instead, a significant source of powering the turbulent velocities in the marginally stable high-z disks is attributed to gravitational instabilities.

Figure 2 illustrates that the observed increase in the intrinsic velocity dispersion with redshift is reminiscent of recent results obtained from Galactic star-by-star archeology and fossil record studies exploiting 3D imaging spectroscopy of a well-resolved individual nearby disk galaxy. In the latter two cases, older stellar populations are associated with progressively thicker disk structures, with a continuum in stellar ages correlating with the vertical velocity dispersion of the respective mono-age stellar population.

It is tempting to associate the similarity to the lookback survey results as an indication that the thicker disk structures were formed as such, from the more gas-rich and turbulent early disks, rather than formed thin and puffed up at a later stage by disturbances such as merger events. Here, again, the caveat applies that in order to consolidate such an

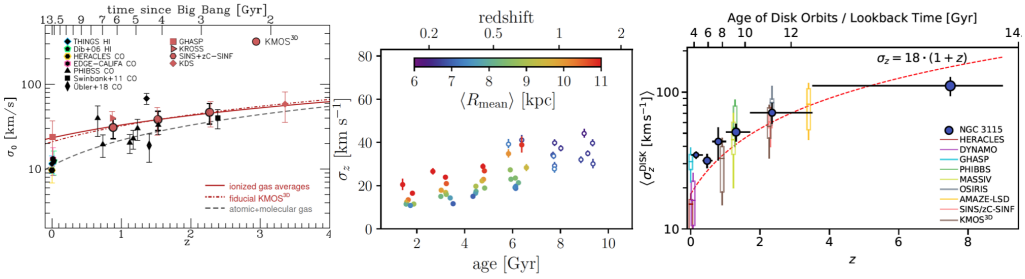

Figure 2. *From left to right:* Intrinsic velocity dispersion of ionized and cold gas as a function of redshift (reproduced from Übler et al. 2019); Galactic vertical velocity dispersion as a function of stellar age (reproduced from Mackereth et al. 2019); Vertical velocity dispersion as a function of age of disk orbits in NGC3115 (reproduced from Poci et al. 2019).

interpretation progenitor and descendant galaxies need to be linked up properly. For the high-redshift studies, this generally requires a push to more adaptive optics assisted observations of low-mass galaxies, enabled by ERIS on VLT and in future years JWST as well as ELT.

Indirect probes of feedback: metallicity gradients. Theoretical models of galaxy formation require strong feedback to resolve the long-standing angular momentum problem (Navarro & Steinmetz 2000), prevent the overproduction of stars and reproduce realistic quenched fractions as a function of galaxy mass and cosmic time. Seeing the imprint of such strong feedback observationally is an area where IFU spectrographs can make unique contributions. In an indirect manner, the fact that the metallicity gradients inferred from ionized gas line ratios are found to be weak, if not flat, on average for SFGs at cosmic noon suggests a continuous mixing of ISM material (Wuyts et al. 2016b; Förster Schreiber et al. 2018). In the absence of injections of energy and momentum, the inside-out growth of stellar disks combined with the chemical enrichment they bring about would otherwise soon lead to the emergence of declining radial profiles in the gas-phase metallicity. Zooming out beyond the disk regions into the Circum-Galactic Medium (CGM), sightline studies by Steidel et al. (2010) have demonstrated the presence of metals at impact parameters beyond 60 kpc. By lack of in situ enrichment so far into the halo the observed metal columns can only be explained by powerful galactic-scale outflows.

Direct probes of feedback: galactic winds. Capturing the launching of such winds can be achieved by decomposing emission line profiles into a systemic and high-velocity component (e.g., Förster Schreiber et al. 2019), a technique complementary to that tracing velocity offsets of interstellar absorption lines which shed light on the neutral phase of the outflow (e.g., Shapley et al. 2003). To this end, IFU data sets offer the unique advantage that the resolved velocity field can be taken out, thereby reducing the width of the systemic component and hence enhancing the contrast with the broad velocity component representing non-gravitational motions. Numbers, depth and dynamic range in galaxy properties sampled by surveys such as KMOS^{3D} have recently brought studies in this area to a stage where not only the occurence of this phenomenon can be established, but its demographics can be mapped across the SFR - mass plane and its energetics and scaling relations can be compared to those predicted by theoretical models. Förster Schreiber et al. (2019) make the case that the outflow phenomenology is best studied for galaxies featuring/lacking diagnostics of AGN activity separately, as their respective broad components differ in characteristic width (FWHM $\sim 400 - 600$ km s^{-1} for star formation driven winds versus FWHM $\sim 1000 - 2500$ km s^{-1} for those emerging from galaxies hosting AGN) and in their demographics. Star formation driven winds are most

prevalent in galaxies residing above the star-forming main sequence, where the highest star formation surface densities (and hence highest energy and momentum injection rates from supernovae) are found. The AGN driven winds on the other hand show a steep mass dependence, becoming increasingly common as one considers galaxies above the Schechter mass, irrespective of their level of star formation activity. Moreover, the inferred energetics are such that much of the material launched by stellar feedback may not make it out of the parent halo and is anticipated to rain back in the form of a galactic fountain. Conversely, the strong outflows emerging from AGN-hosting galaxies at the high-mass end may do more (long-term) damage to the gas reservoirs.

4. Outlook and open questions

Deep multi-wavelength lookback surveys combined with integral-field spectroscopy and accumulating resolved CO data sets are providing a rich multi-tracer view on the nature of gas-rich disk galaxies at cosmic noon. The large multiplexing of new near-infrared (and particularly IFU) spectrographs has enabled placing early results gathered painstakingly by observing of order 1 galaxy per observing night on an 8m-class telescope on a more robust statistical footing. In addition, recent results also prompt a new array of questions:

- *What is the origin of 'unphysical' baryon fractions ($M_{\rm bar}/M_{\rm dyn} > 1$)?* A robust trend of increasing baryon fractions with increasing surface density is emerging from disk modeling of IFU kinematics. At its extremes, the number of galaxies for which the baryonic mass enclosed within R_e exceeds the dynamical constraint $M_{\rm dyn}(< R_e)$ appears larger than what can be accounted for by random uncertainties. Are these compact SFGs closer to being gas depleted than conventional gas scaling relations, established for the bulk of the galaxy population, suggest? Are uncertainties on their dynamical masses underestimated (e.g., because in the most extreme cases axial ratio based inclinations are hard to determine accurately for marginally resolved compact nuggets)? Or do they represent a subpopulation for which treatment with thick disk models becomes inadequate?
- *What is the physics responsible for setting σ_0?* The redshift evolution of σ_0 can be understood in the framework of marginally stable disks with gas fractions that are dwindling with cosmic time (Wisnioski et al. 2015; Übler et al. 2019). Yet, at fixed redshift no statistically significant relations between σ_0 and for example the gas fraction within galaxies can be discerned within current data sets. Is this because the dynamic range sampled at a given epoch is modest, and measurement uncertainties in the relevant quantities (σ_0, $f_{\rm gas}$) comparatively large? Or are we missing physics? Furthermore, nearby galaxies are known to feature velocity anisotropies with radial velocity dispersions σ_R typically exceeding those measured along the axis orthogonal to the disk plane. In contrast, the assumption of an isotropic velocity ellipsoid (i.e., $\sigma_0 = \sigma_R = \sigma_z$) is commonly adopted in the analysis of high-z kinematics.
- *What are the total mass loading and energetics of galactic-scale winds and how does it break down into multi-phase components?* Much of what was discussed above in terms of wind properties and demographics was based on the ionized phase only. A more holistic view on wind properties and their impact on a galaxy's evolutionary path requires the combination of multi-phase tracers. To date, the number of individual normal main sequence SFGs (as opposed to luminous starbursting outliers or extreme quasars) with wind properties mapped in the neutral phase through interstellar absorption line shifts, as well as in the ionized and molecular phase through broad components to the [OIII] or Hα and CO emission lines, remains extremely small. A pilot programme by Herrera-Camus et al. (2019) suggests that, equivalent to what is seen in nearby starbursts, the bulk of the mass flow may be in the molecular phase, implying that ionized gas observations alone are insufficient to fully capture their impact on galaxy evolution.

New facilities coming online this decade, such as ERIS on VLT, JWST and ELT, further promise to advance our knowledge on not only gas but also stellar kinematics within distant SFGs, and on anticipated deviations from circular motions enabling tests of in situ bulge formation scenarios in which radial gas flows result from violent disk instabilities.

References

Belli, S., Newman, A. B., & Ellis, R. S. 2017, *ApJ*, 834, 18
Bezanson, R., van der Wel, A., Pacifici, C., et al. 2018, *ApJ*, 858, 60
Brammer, G. B., van Dokkum, P. G., & Coppi, P. 2008, *ApJ*, 686, 1503
Bullock, J. S., Dekel, A., Kolatt, T. S., et al. 2001, *ApJ*, 555, 240
Burkert, A., Förster Schreiber, N. M., Genzel, R., et al. 2016, *ApJ*, 826, 214
Burkert, A., Genzel, R., Bouché, N., et al. 2010, *ApJ*, 725, 2324
Chang, Y.-Y., van der Wel, A., Rix, H.-W., et al. 2013, *ApJ*, 762, 83
Courteau, S., & Dutton, A. A. 2015, *ApJ*, 801, 20
Cresci, G., Hicks, E. K. S., Genzel, R., et al. 2009, *ApJ*, 697, 115
Davidzon, I., Ilbert, O., Laigle, C., et al. 2017, *A&A*, 605, 70
Förster Schreiber, N. M., Renzini, A., Mancini, C., et al. 2018, *ApJS*, 238, 21
Förster Schreiber, N. M., Übler, H., Davies, R. L., et al. 2019, *ApJ*, 875, 21
Genzel, R., Förster Schreiber, N. M., Übler, H., et al. 2017, *Nature*, 543, 397
Herrera-Camus, R., Tacconi, L., Genzel, R., et al. 2019, *ApJ*, 871, 37
Huang, K.-H., Fall, S. M., Ferguson, H. C., et al. 2017, *ApJ*, 838, 6
Johnson, H. L., Harrison, C. M., Swinbank, A. M., et al. 2018, *MNRAS*, 474, 5076
Kravtsov, A. V. 2013, *ApJ*, 764, 31
Krumholz, M. R., Burkhart, B., Forbes, J. C., & Crocker, R. M. 2018, *MNRAS*, 477, 2716
Lang, P., Förster Schreiber, N. M., Genzel, R., et al. 2017, *ApJ*, 840, 92
Mackereth, J. T., Bovy, J., Leung, H. W., et al. 2019, *MNRAS*, in press (arXiv1901.04502)
Poci, A., McDermid, R. M., Zhu, L., & van de Ven, G. 2019, *MNRAS*, 487, 3776
Mo, H. J., Mao, S., & White, S. D. M. 1998, *MNRAS*, 295, 319
Mowla, L., van der Wel, A., van Dokkum, P. G., & Miller, T. B. 2019, *ApJ*, 872, 13
Navarro, J. F., & Steinmetz, M. 2000, *ApJ*, 538, 477
Newman, A. B., Belli, S., & Ellis, R. S. 2015, *ApJ*, 813, 7
Newman, A. B., Belli, S., Ellis, R. S., & Patel, S. G. 2018, *ApJ*, 862, 126
Robertson, B., Bullock, J. S., Cox, T. J., et al. 2006, *ApJ*, 645, 986
Sanders, R. L., Shapley, A. E., Kriek, M., et al. 2018, *ApJ*, 858, 99
Shapley, A. E., Steidel, C. C., Pettini, M., & Adelberger, K. L. 2003, *ApJ*, 588, 65
Speagle, J. S., Steinhardt, C. L., Capak, P. L., & Silverman, J. D. 2014, *ApJS*, 214, 15
Steidel, C. C., Erb, D. K., Shapley, A. E., et al. 2010, *ApJ*, 717, 289
Tacconi, L. J., Genzel, R., Saintonge, A., et al. 2018, *ApJ*, 853, 179
Tiley, A. L., Swinbank, A. M., Harrison, C. M., et al. 2019, *MNRAS*, 485, 934
Toft, S., Zabl, J., Richard, J., et al. 2017, *Nature*, 546, 510
Übler, H., Förster Schreiber, N. M., Genzel, R., et al. 2017, *ApJ*, 842, 121
Übler, H., Genzel, R., Wisnioski, E., et al. 2019, *ApJ*, 880, 48
van der Wel, A., Rix, H.-W., Wuyts, S., et al. 2011, *ApJ*, 730, 38
van der Wel, A., Franx, M., van Dokkum, P. G., et al. 2014, *ApJ*, 788, 28
Wellons, S., Torrey, P., Ma, C.-P., et al. 2015, *MNRAS*, 449, 361
Wisnioski, E., Förster Schreiber, N. M., Wuyts, S., et al. 2015, *ApJ*, 799, 209
Wisnioski, E., Förster Schreiber, N. M., Fossati, M., et al. 2019, *ApJ*, submitted
Wuyts, S., Cox, T. J., Hayward, C., et al. 2010, *ApJ*, 722, 1666
Wuyts, S., Förster Schreiber, N. M., van der Wel, A., et al. 2011, *ApJ*, 742, 96
Wuyts, S., Förster Schreiber, N. M., Wisnioski, E., et al. 2016, *ApJ*, 831, 149
Wuyts, E., Wisnioski, E., Fossati, M., et al. 2016, *ApJ*, 827, 74
Zanisi, L., Shankar, F., Lapi, A., et al. 2019, *MNRAS*, submitted